A Three-dimensional Spatiotemporal Model for Remote Sensing Data Cubes

Fábio M. Bayer
Departamento de Estatística
Universidade Federal de Santa Maria - UFSM
bayer@ufsm.br

Joint work with
Débora M. Bayer (UFSM), Paolo Gamba (UNIPV).

PIPGES/UFSCar-USP

Motivação

Sinal unidimensional (1D)

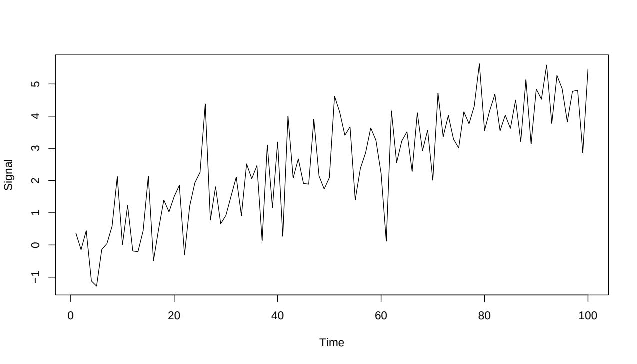

Figure 1: Exemplo de sinal unidimensional (série temporal).

- Modelos ARMA para séries temporais (jargão da estatística)
- Filtro ARMA para sinais (jargão de processamento de sinais)

Motivação

Sinal bidimensional (2D)

(a) Lena (b) Pixels

Figure 2: Exemplo de sinal bidimensional (imagem).

- Modelos ARMA espaciais ou bidimensionais

Motivação

Sinal tridimensional (3D)

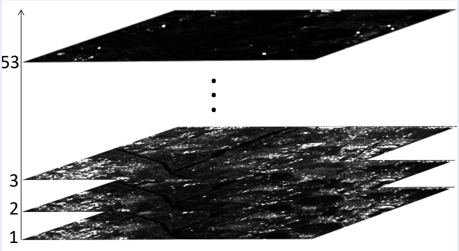

Figure 3: Série temporal de imagens de radar de abertura sintética (SAR).

- Modelos ARMA tridimensionais????

Introduction

Time series of satellite images are important sources for satellite data interpretation and Earth monitoring [1, 2, 3].

This type of data has been increasingly available with high temporal and spatial resolutions [1], offering a wide range of Earth observation (EO) applications, such as:

- land-use classification [4, 5],
- change detection [6, 7],
- filtering [8, 9],
- missing information reconstruction [10, 11, 12].

Introduction

Spatio-temporal satellite data can be mathematically described as a three-dimensional (3D) array, or a 3D cube.

The technical literature is populated by techniques to handle this type of data. In general, these works consider:

(i) unidimensional (1D) pixel-based approaches [13, 14, 15, 16, 6], ignoring the spatial correlation,

(ii) time-by-time spatial techniques [17, 18, 19], ignoring the temporal correlation.

Some options for modeling these data types: 1D ARMA models [20, 21] and spatial ARMA models [22, 23, 24, 25, 26].

These models and their statistical inference techniques, including robust estimation [27, 22, 23], are explored in different image processing applications.

Introduction

To the best of our knowledge, a 3D autoregressive (AR) statistical model, as a generalization of the above-mentioned 1D and 2D models to the third dimension, is absent in the literature.

Thus, we attempt to fulfill this gap by proposing a parametric 3D statistical model for multitemporal satellite image interpretation that considers spatial and time correlations in the same AR framework.

We introduce the proposed 3D-AR dynamical model and discuss parameter estimation.

The results show that the proposed model can be used for filtering, gap-filling, anomaly detection, and future prediction in a multitude of sensors and EO applications.

Introduction

As remote sensing data usually contain anomalous values (outliers) [28] (clouds, land contamination, sensor failures), this work introduces a **robust method** for the estimation of the 3D-AR model parameters.

Specifically, weighted least square estimators (WLSE) [27] are considered.

Additionally, this work introduces filtering and prediction methods, as well as residuals and anomaly detection techniques.

The residual-based control charts [29] can be used to detect anomalous areas, which in turn may be due to multiple phenomena, such as deforestation, droughts, fires, clouds, plant phenological cycles, or even sensor failures.

The Proposed 3D Model

A multi-temporal geometrically and radiometrically corrected remote sensing image stack can be defined as a 3D cube $\mathbf{Y}$ of size $M \times N \times T$.

Let the voxel $Y[m, n, t] \in \mathbf{Y}$ be a random variable, with $(m, n, t) \in \mathbb{Z}^3$, where $m = 1, \ldots, M$ and $n = 1, \ldots, N$ are the spatial dimensions and $t = 1, \ldots, T$ is the time dimension.

Each voxel of the 3D cube can be written as

$$Y[m, n, t] = \mu[m, n, t] + \varepsilon[m, n, t], \tag{1}$$

where $\mu[m, n, t]$ is the mean of $Y[m, n, t]$ and $\varepsilon[m, n, t]$ are independent random variables with $\mathrm{E}(\varepsilon[m, n, t]) = 0$ and $\mathrm{Var}(\varepsilon[\mathrm{m}, \mathrm{n}, \mathrm{t}]) = \sigma^2$.

In order to represent the 3D cube using a statistically treatable model, we model the mean of each voxel as a function of some parameters, with the following 3D dynamical general structure:

$$\mu[m,n,t] = \mathbf{x}[m,n,t]^\top \boldsymbol{\beta} + \sum_{i,j,k} \phi_{(i,j,k)} y[m-i, n-j, t-k], \qquad (2)$$

where $y[m,n,t]$ is an observed value of the random variable $Y[m,n,t]$ at $[m,n,t]$, $\mathbf{x}[m,n,t] = (x_1[m,n,t], \ldots, x_r[m,n,t])^\top$ is a r-dimensional vector of covariates (non-random input variables), $\boldsymbol{\beta} = (\beta_1, \ldots, \beta_r)^\top$ is the r-dimensional vector of unknown parameters related to covariates, $\phi_{(i,j,k)}$ are the unknown autoregressive (AR) parameters of the model, and $(m-i, n-j, t-k)$ belongs to some determined support or **neighborhood of the model** $\mathcal{N}_{\{m,n,t\}}$.

The covariates can be used to model inhomogeneous images, with different types of land use or seasonality patterns, for example.

There are several possibilities to consider for the neighborhood $\mathcal{N}_{\{m,n,t\}}$, and they have been investigated in technical literature especially for the two-dimensional (2D) case [30, 31, 22, 25].

Motivated by the physical acquisition of the time series satellite images and for parsimonious reason, we define the neighbor structure as the set of past values of $t \in \mathbb{Z}$, i.e., the set of images observed until the current time stamp t. Mathematically, let's define this neighborhood as $\mathcal{N}_{\{m,n,t\}} = \{(i,j,k) \in \mathbb{Z}^3 : k < t\}$.

Thus results into 3D-AR structure of order p, called 3D-AR(p), given by:

$$\mu[m,n,t] = \mathbf{x}[m,n,t]^\top \boldsymbol{\beta} + \sum_{k=1}^{p} \sum_{j=1}^{2k+1} \sum_{i=1}^{2k+1} \phi_{(i,j,k)} \times y[m-(k+1)+i, n-(k+1)+j, t-k], \tag{3}$$

with $g = \sum_{k=1}^{p}(2k+1)^2$.

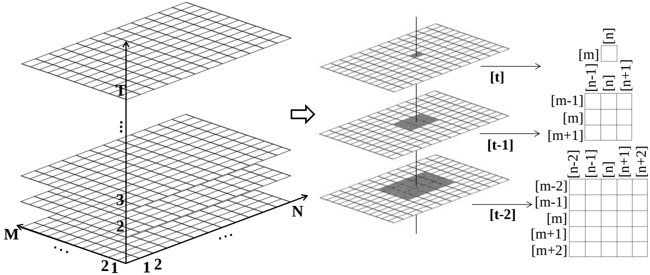

Figure 4: 3D-AR(2) model scheme. The voxels at instant t are written as linear combination of the hatched voxels at instants $t-1$ and $t-2$.

Robust Estimation

Given a 3D data cube of satellite observations, the problem is to estimate the vector of parameters $\gamma = (\boldsymbol{\beta}^\top, \boldsymbol{\phi}^\top)^\top$.

The traditional least square estimator (LSE) could be an option, but it is highly sensitive to outliers [27].

Outliers can be defined as anomalous values with respect to the surrounding pixels (2D case) [28] or voxels (3D case).

Remote sensing image stack often contain outliers [32, 28].

In these cases, robust methods [27], such as the weighted least square estimation (WLSE), can be a good choice to obtain inferences less sensitive to outliers.

Robust Estimation

The WLSE $\hat{\gamma}$ of the 3D-AR(p) model parameters γ is thus obtained by equating the derivatives to zero and solving the system.

Using similar results from [27], this solution presents the following matrix closed form:

$$\hat{\gamma} = \left(\mathbf{Z}^\top \mathbf{W} \mathbf{Z}\right)^{-1} \mathbf{Z}^\top \mathbf{W} \mathbf{y},$$

where $\mathbf{y} = (y[1+p, 1+p, 1+p], \ldots, y[M-p, 1+p, 1+p], y[1+p, 2+p, 1+p], \ldots, y[M-p, 2+p, 1+p], \ldots, y[1+p, N-p, 1+p], \ldots, y[M-p, N-p, 1+p], y[1+p, 1+p, 2+p], \ldots, y[M-p, N-p, T])$,
$\mathbf{W} = \operatorname{diag}\left(w[1+p, 1+p, 1+p], \ldots, w[M-p, 1+p, 1+p], w[1+p, 2+p, 1+p], \ldots, w[M-p, 2+p, 1+p], \ldots, w[M-p, N-p, 1+p], w[1+p, 1+p, 2+p], \ldots, w[M-p, N-p, T]\right)$.

Robust Estimation

The estimation procedure could be computationally cumbersome for big data cubes, being restrictive for applications in platforms with limited performance.

However, a smaller data cube can be used only for parameter estimation.

Our simulation results suggest that cubes with dimension about $20 \times 20 \times 30$ present good estimates.

Even if the parameter estimates are extracted from a smaller cube it is then possible to apply the filtering, prediction, and anomaly detection techniques discussed in the following to the whole original 3D cube.

Filtering and Prediction

The filtered signal is given by the estimated values of $\mu[m, n, t]$, given by the 3D dynamical structure in (3) evaluated at the WLSE $\hat{\gamma}$. Accordingly:

$$\hat{\mu}[m, n, t] = \mathbf{x}[m, n, t]^\top \hat{\beta} + \sum_{k=1}^{p} \sum_{j=1}^{2k+1} \sum_{i=1}^{2k+1} \hat{\phi}_{(i,j,k)} \tag{4}$$

$$\times \{y[m-(k+1)+i, n-(k+1)+j, t-k]\}_f \,,$$

where

$$\{y[m, n, t]\}_f = \begin{cases} \hat{\mu}[m, n, t], & \text{if } F(m, n, t) < \delta \\ y[m, n, t], & \text{if } \delta \leqslant F(m, n, t) \leqslant 1-\delta \,. \\ \hat{\mu}[m, n, t], & \text{if } F(m, n, t) > 1-\delta \end{cases} \tag{5}$$

Note that in (5), when $y[\cdot, \cdot, t]$ is an outlier it is not considered for the estimate of $\mu[\cdot, \cdot, t+k]$, with $k = 1, \ldots, p$. In these cases, instead of using the anomalous values $y[m, n, t]$, the estimated values $\hat{\mu}[m, n, t]$ are used.

Filtering and Prediction

The filtered scheme in (4) presents some problems at the border of the 3D cube.

To avoid these issues, a half padding procedure [33] in the spatial dimensions is used (Fig 5(a)), as well as back-calculation values for the first p times (Fig 5(b)).

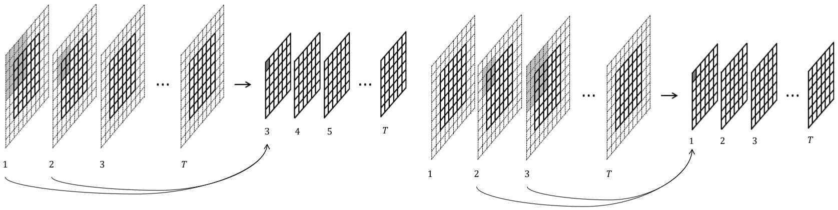

(a) Half pading spatial convolution

(b) Back-calculation in time

Figure 5: 3D-AR(2) model convolution scheme. The observed 3D cube is represented to the left and the filtered image to the right.

Residual Analysis and Anomaly Detection

A residual analysis is used as an assessment criteria for the goodness-of-fit of the fitted 3D-AR(p) model.

We consider the standardized residual given by

$$r[m,n,t] = \frac{y[m,n,t] - \hat{\mu}[m,n,t]}{\hat{\sigma}}. \tag{6}$$

If the model is correctly specified, the standardized residuals are approximately Gaussian distributed with zero mean and unit variance, i.e., $r[m,n,t] \sim N(0,1)$.

Residual Analysis and Anomaly Detection

The formulation of the 3D-AR(p) model enables anomaly detection by considering residuals monitoring based on the classical theory of control charts [29].

Specifically in the framework of this research, the 3D-AR residual-based control charts may be used to detect anomalous areas in 3D data cubes:

1. For each residual voxel $r[m, n, t]$ verify if $-3 < r[m, n, t] < 3$.
2. Create a binary cube with value 1 if the residual voxel is outside of the interval $(-3, 3)$ and 0 otherwise.
3. Apply dilation-erosion morphological operations on the binary cube. (usual image processing operations)

Residual Analysis and Anomaly Detection

The formulation of the 3D-AR(p) model enables anomaly detection by considering residuals monitoring based on the classical theory of control charts [29].

Specifically in the framework of this research, the 3D-AR residual-based control charts may be used to detect anomalous areas in 3D data cubes:

1. For each residual voxel $r[m, n, t]$ verify if $-3 < r[m, n, t] < 3$.
2. Create a binary cube with value 1 if the residual voxel is outside of the interval $(-3, 3)$ and 0 otherwise.
3. Apply dilation-erosion morphological operations on the binary cube. (usual image processing operations)

Simulation Study

In this section we evaluate the performance of the point estimators of the 3D-AR model parameters through a Monte Carlo simulation.

All implementations and simulations were carried out using the `R` language [34].

The synthetic spatio-temporal images were generated as a 3D cube following the 3D-AR structure given by (1) and (3), where the error terms $\varepsilon[m, n, t]$ in (1) are simulated from zero mean normal distribution.

Simulation Study

A 3D-AR(1) with one deterministic covariate was simulated with the following parameter values: $\beta_1 = 0.06$, $\phi_{1,1,1} = 0.19$, $\phi_{2,1,1} = 0.07$, $\phi_{3,1,1} = 0.21$, $\phi_{1,2,1} = 0.03$, $\phi_{2,2,1} = -0.02$, $\phi_{3,2,1} = 0.02$, $\phi_{1,3,1} = 0.15$, $\phi_{2,3,1} = 0.06$, and $\phi_{3,3,1} = 0.17$.

Two dispersion parameter values are considered, namely: $\sigma = 0.24$ and $\sigma = 1$.

The parameter values are based on the fitted 3D-AR(1) model for the actual NDVI times series in the following.

To mimic a seasonality pattern in the signal, the covariate are considered as $x_1[\cdot, \cdot, t] = \cos(2\pi t/12)$, with $t = 1, \ldots, T$.

The dimensions of the 3D cubes were set to $20 \times 20 \times T$, with $T \in \{10, 20, 30\}$.

We set $\delta = 0.01$ for weights determination, which proved a suitable choice based on previews experiments and simulations.

Simulation Study

In order to evaluate the LSE and its robust version WLSE, the mean, bias, percentage relative bias (RB%), and mean square error (MSE) of the estimators were computed, based on 500 replications of the 3D signal.

For this evaluation we considered two approaches: 3D signal generated with outliers and without outliers.

Specifically, to include outliers, we added the value four in 5% of the voxels in randomized positions.

The results with and without outliers are shown in two tables. (omitted in this presentation)

Results: We can note that, in general, the WLSE present smaller MSE values than LSE.

Simulation Study

In order to evaluate the LSE and its robust version WLSE, the mean, bias, percentage relative bias (RB%), and mean square error (MSE) of the estimators were computed, based on 500 replications of the 3D signal.

For this evaluation we considered two approaches: 3D signal generated with outliers and without outliers.

Specifically, to include outliers, we added the value four in 5% of the voxels in randomized positions.

The results with and without outliers are shown in two tables. (omitted in this presentation)

Results: We can note that, in general, the WLSE present smaller MSE values than LSE.

Simulation Study

In order to evaluate the LSE and its robust version WLSE, the mean, bias, percentage relative bias (RB%), and mean square error (MSE) of the estimators were computed, based on 500 replications of the 3D signal.

For this evaluation we considered two approaches: 3D signal generated with outliers and without outliers.

Specifically, to include outliers, we added the value four in 5% of the voxels in randomized positions.

The results with and without outliers are shown in two tables. (omitted in this presentation)

Results: We can note that, in general, the WLSE present smaller MSE values than LSE.

Simulation Study

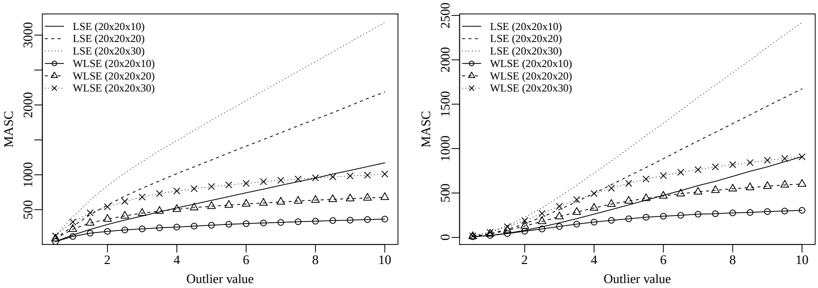

(a) $\sigma = 0.24$ (b) $\sigma = 1.00$

Figure 6: Sensitivity results for two different variance scenarios.

The visual results show that the WLSE is less sensitive to outliers than LSE for all outlier values in all cases.

Simulation Study

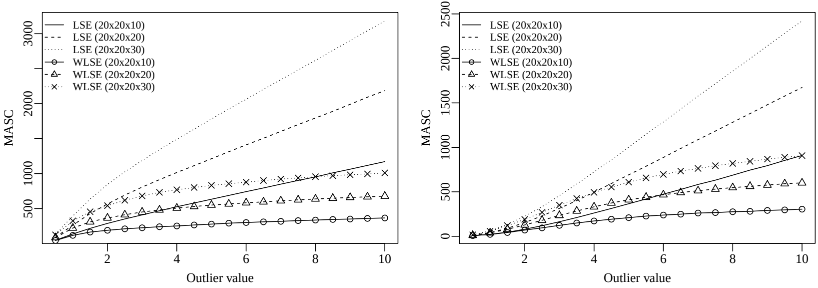

(a) $\sigma = 0.24$ (b) $\sigma = 1.00$

Figure 6: Sensitivity results for two different variance scenarios.

The visual results show that the WLSE is less sensitive to outliers than LSE for all outlier values in all cases.

Multitemporal NDVI Data Interpretation

In order to show the applicability of the proposal for modeling, predicting, and detecting anomalies in 3D remote sensing data cubes, the 3D-AR model will be applied to a spatio-temporal NDVI dataset.

The multitemporal data used in this work is composed by 33 100×100 NDVI images observed between February 2018 and June 2019 over the Paraíba State, Brazil.

The NDVI data for this location are composed over approximately 15 days periods with 250 meters of spatial resolution.

These NDVI images are from NASA Earth Observing System (EOS), and they are part of moderate resolution imaging spectroradiometer (MODIS) collection.

Multitemporal NDVI Data Interpretation

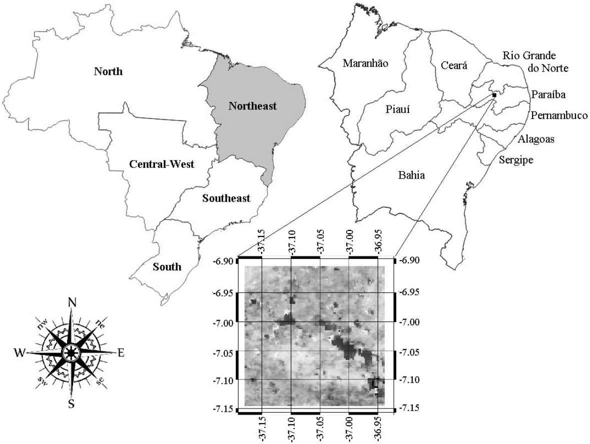

Figure 7: Aerial view of considered area.

Multitemporal NDVI Data Interpretation

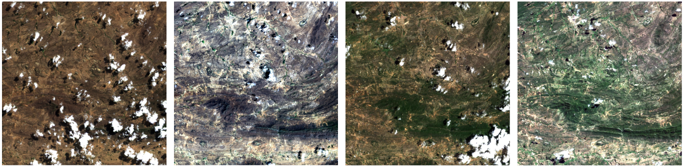

(a) Aug 2018 (b) Nov 2018 (c) Feb 2019 (d) May 2019

Figure 8: Optical Landsat-8 (RGB; 432) image shows the study area in different periods of the year.

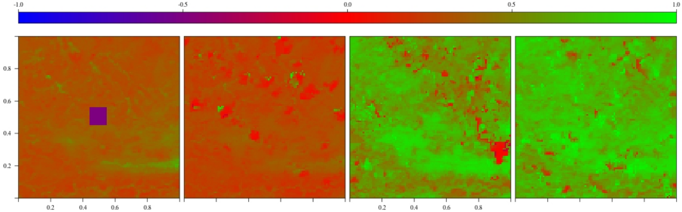

Figure 9: Quarterly NDVI observation images.

Multitemporal NDVI Data Interpretation

For parameter estimation purpose only, we selected a smaller cube with $40 < m < 60$, $40 < n < 60$, and $1 < t < 33$.

In addition, a square of synthetic outliers (synthetic anomalous observations) was added to the signal.

We arbitrary consider this inclusion at time $t = 14$ in the pixels with $45 < m < 55$ and $45 < n < 55$.

We replaced the observed values of these voxels by -0.5. This negative value can represent, for example, a thick cloud.

Multitemporal NDVI Data Interpretation

This synthetic inclusion has three main aims, namely:

(i) to evaluate the performance of the robust estimation procedure in the presence of atypical values,

(ii) to check the filtering performances on a real data set with some exogenous intervention,

(iii) to verify the performance of the anomaly detection technique.

Multitemporal NDVI Data Interpretation

To account for seasonality along the determined period, we considered the covariate $x_1[\cdot,\cdot,t] = \cos(2\pi(t+18)/24)$ that consists of 24 biweekly observations for each year.

The fitted 3D-AR(1) model has the following estimated parameter values: $\hat{\sigma} = 0.2442$, $\hat{\beta}_1 = 0.0570$, $\hat{\phi}_{(1,1,1)} = 0.1913$, $\hat{\phi}_{(2,1,1)} = 0.0734$, $\hat{\phi}_{(3,1,1)} = 0.2126$, $\hat{\phi}_{(1,2,1)} = 0.0295$, $\hat{\phi}_{(2,2,1)} = -0.0250$, $\hat{\phi}_{(3,2,1)} = 0.0201$, $\hat{\phi}_{(1,3,1)} = 0.1483$, $\hat{\phi}_{(2,3,1)} = 0.0642$, and $\hat{\phi}_{(3,3,1)} = 0.1710$.

Figure 10 shows that the residuals are normally distributed around zero and most of them are in the interval $(-3, 3)$.

Multitemporal NDVI Data Interpretation

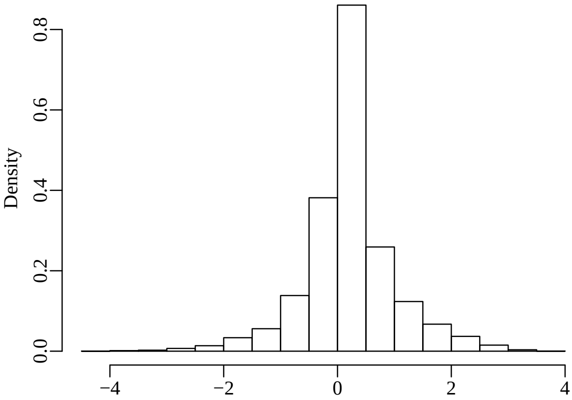

Figure 10: Histogram of residuals.

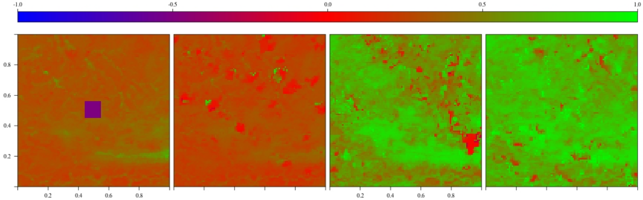
-1.0
-0.5
0.0
0.5
1.0
0.8
0.6
0.4
0.2
0.2
0.4
0.6
0.8

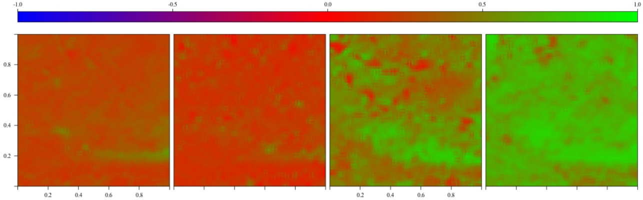
-1.0
-0.5
0.0
0.5
1.0
0.8
0.6
0.4
0.2
0.2
0.4
0.6
0.8

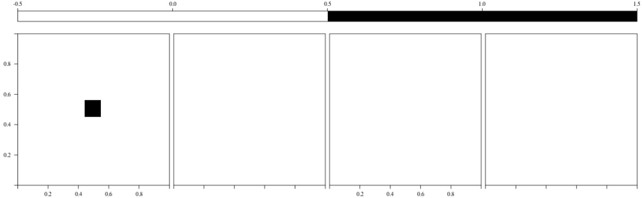
-0.5
0.0
0.5
1.0
1.5
0.8
0.6
0.4
0.2
0.2
0.4
0.6
0.8

Multitemporal NDVI Data Interpretation

- The filtered images show that the model is able to capture the main patterns of the observed signal, smoothing variability and gap-filling the outliers in the squared region.
- The proposed residual-based anomaly detection technique is effective in detecting anomalies in multitemporal data.
- After morphological operations, only the included synthetic gap is detected.

Multitemporal NDVI Data Interpretation

For comparison purposes, we also fitted unidimensional first order autoregressive (AR(1)) models pixel by pixel.

This approach was suggested by [6] for prediction and change detection applications in multitemporal SAR images. We used the `R` package `forecast` [35] to fit the AR(1) model.

Table 1: Comparison measures for 3D-AR and unidimensional AR models fitted to NDVI data (best figures in bold)

Model	r	MAPE	time (sec)
3D-AR (proposed)	**0.57**	**0.54**	**41.23**
AR (pixel by pixel)	0.56	0.60	58.36

Multitemporal NDVI Data Interpretation

A pixel-based visual analysis of a few spatial points is also presented.

The filtered values by the proposed 3D model are closer to the observed ones than the 1D approach.

The included outliers do not influence next filtered values, evidencing the robustness of the 3D-AR model.

The predictions based on the proposed model better capture the seasonal behavior of the signal, useful for future decision making.

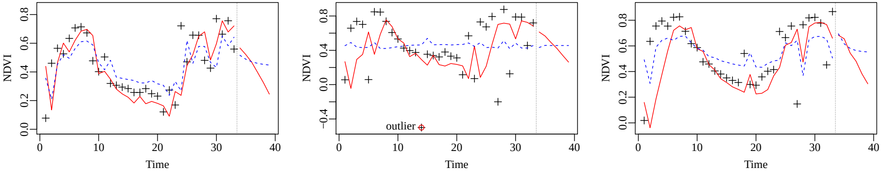

Figure 11: Observed (points) unidimensional time series for pixels $[25, 25]$, $[50, 50]$, $[75, 75]$, and their filtered values considering the 3D-AR(1) model (continuous line) and unidimensional AR(1) model (dashed lines).

Multitemporal NDVI Data Interpretation

Some land cover works are interested to the percentage of vegetation in a certain scene [36, 37].

We analyzed the percentages of observed and filtered NDVI values over 0.3, 0.5, and 0.7 thresholds.

The proposed model shows very similar percentages between observed and filtered values.

These prediction results could be useful for a multitude of applications, such as input of deterministic and stochastic models, from hydrology to epidemiology.

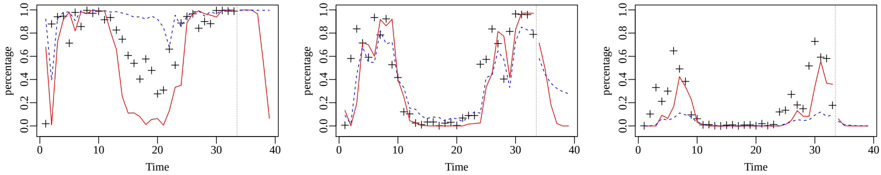

Figure 12: Percentage of NDVI values greater than 0.3, 0.5, and 0.7 over time.

Conclusion

This paper proposes a 3D dynamical model for the interpretation of multi-temporal remote sensing images.

Tools for parameter estimation, filtering, prediction, and anomaly detection obtained from the models were also discussed.

As outliers are often present in remote sensing images, the weighted least square estimation was considered as a robust alternative for parameter estimation.

A simulation study was carried out for point estimation evaluation. The simulation results validates the inference procedures.

Conclusion

Since the model is useful to model signals that can be described as a 3D cube, an application to an NDVI data cube was performed.

The NDVI test show that the proposed 3D-AR model is able to model the pattern of the time series, providing accurate filtered signals and predicted values.

It was also capable to detect exogenous artifacts such as thick clouds or sensor failures.

The numerical experiments show the flexibility and usefulness of the proposed model to model 3D data cubes.

Indeed, the proposed model is general enough to model other types of 3D structures, such as hyperspectral images [38] and 3D heightmap, where the third dimension is the wavelength in the former and the altitude in the latter.

References I

F. Petitjean, J. Inglada, and P. Gancarski, “Satellite image time series analysis under time warping,” *IEEE Transactions on Geoscience and Remote Sensing*, vol. 50, no. 8, pp. 3081–3095, 2012.

L. Poggio, A. Gimona, and I. Brown, “Spatio-temporal MODIS EVI gap filling under cloud cover: An example in Scotland,” *ISPRS Journal of Photogrammetry and Remote Sensing*, vol. 72, pp. 56–72, 2012.

L. Xu, B. Li, Y. Yuan, X. Gao, and T. Zhang, “A temporal-spatial iteration method to reconstruct NDVI time series datasets,” *Remote Sensing*, vol. 7, no. 7, pp. 8906–8924, 2015.

K.-F. Lin and D. Perissin, “Single-polarized SAR classification based on a multi-temporal image stack,” *Remote Sensing*, vol. 10, no. 7, 2018.

A. Marinoni, G. C. Iannelli, and P. Gamba, “An information theory-based scheme for efficient classification of remote sensing data,” *IEEE Transactions on Geoscience and Remote Sensing*, vol. 55, no. 10, pp. 5864–5876, 2017.

B. G. Palm, D. I. Alves, V. T. Vu, M. I. Pettersson, F. M. Bayer, R. J. Cintra, R. Machado, P. Dammert, and H. Hellsten, “Autoregressive model for multi-pass SAR change detection based on image stacks,” in *SPIE Image and Signal Processing for Remote Sensing XXIV*, vol. 10789, 2018.

References II

C. Marin, F. Bovolo, and L. Bruzzone, "Building change detection in multitemporal very high resolution SAR images," *IEEE Transactions on Geoscience and Remote Sensing*, vol. 53, no. 5, pp. 2664–2682, 2015.

T. T. Lê, A. M. Atto, E. Trouvé, and J. Nicolas, "Adaptive multitemporal SAR image filtering based on the change detection matrix," *IEEE Geoscience and Remote Sensing Letters*, vol. 11, no. 10, pp. 1826–1830, 2014.

J. Yuan, X. Lv, and R. Li, "A speckle filtering method based on hypothesis testing for time-series SAR images," *Remote Sensing*, vol. 10, no. 9, 2018.

H. Shen, X. Li, Q. Cheng, C. Zeng, G. Yang, H. Li, and L. Zhang, "Missing information reconstruction of remote sensing data: A technical review," *IEEE Geoscience and Remote Sensing Magazine*, vol. 3, no. 3, pp. 61–85, 2015.

Q. Zhang, Q. Yuan, C. Zeng, X. Li, and Y. Wei, "Missing data reconstruction in remote sensing image with a unified spatial–temporal–spectral deep convolutional neural network," *IEEE Transactions on Geoscience and Remote Sensing*, vol. 56, no. 8, pp. 4274–4288, 2018.

Y. Julien and J. A. Sobrino, "Optimizing and comparing gap-filling techniques using simulated NDVI time series from remotely sensed global data," *International Journal of Applied Earth Observation and Geoinformation*, vol. 76, pp. 93–111, 2019.

References III

——, "Global land surface phenology trends from gimms database," *International Journal of Remote Sensing*, vol. 30, no. 13, pp. 3495–3513, 2009. [Online]. Available: https://doi.org/10.1080/01431160802562255

——, "Comparison of cloud-reconstruction methods for time series of composite NDVI data," *Remote Sensing of Environment*, vol. 114, no. 3, pp. 618–625, 2010.

G. J. Roerink, M. Menenti, and W. Verhoef, "Reconstructing cloudfree NDVI composites using Fourier analysis of time series," *International Journal of Remote Sensing*, vol. 21, no. 9, pp. 1911–1917, 2000.

E. B. Brooks, V. A. Thomas, R. H. Wynne, and J. W. Coulston, "Fitting the multitemporal curve: A Fourier series approach to the missing data problem in remote sensing analysis," *IEEE Transactions on Geoscience and Remote Sensing*, vol. 50, no. 9, pp. 3340–3353, 2012.

C. Zhang, W. Li, and D. Travis, "Gaps-fill of SLC-off Landsat ETM+ satellite image using a geostatistical approach," *International Journal of Remote Sensing*, vol. 28, no. 22, pp. 5103–5122, 2007.

H. Shen and L. Zhang, "A MAP-based algorithm for destriping and inpainting of remotely sensed images," *IEEE Transactions on Geoscience and Remote Sensing*, vol. 47, no. 5, pp. 1492–1502, 2009.

References IV

A. Bugeau, M. Bertalmio, V. Caselles, and G. Sapiro, "A comprehensive framework for image inpainting," *IEEE Transactions on Image Processing*, vol. 19, no. 10, pp. 2634–2645, 2010.

G. Box, G. M. Jenkins, and G. Reinsel, *Time Series Analysis: Forecasting and Control*. Hardcover, John Wiley & Sons, 2008.

P. J. Brockwell and R. A. Davis, *Time series: Theory and methods*. New York: Springer-Verlag, 2013.

O. Bustos, S. Ojeda, and R. Vallejosb, "Spatial ARMA models and its applications to image filtering," *Brazilian Journal of Probability and Statistics*, vol. 23, no. 2, pp. 141–165, 2009.

G. M. Britos and S. M. Ojeda, "Robust estimation for spatial autoregressive processes based on bounded innovation propagation representations," *Computational Statistics*, vol. 34, pp. 1315–1335, 2019.

O. H. Bustos, M. Ruiz, S. Ojeda, R. Vallejos, and A. C. Frery, "Asymptotic behavior of RA-estimates in autoregressive 2D processes," *Journal of Statistical Planning and Inference*, vol. 139, no. 10, pp. 3649–3664, 2009.

B. Choi and D. N. Politis, "Modeling 2-D AR processes with various regions of support," *IEEE Transactions on Signal Processing*, vol. 55, no. 5, pp. 1696–1707, 2007.

References V

A. Sarkar, K. Sharma, and R. V. Sonak, “A new approach for subset 2-D AR model identification for describing textures,” *IEEE Transactions on Image Processing*, vol. 6, no. 3, pp. 407–413, 1997.

A. M. Zoubir, V. Koivunena, E. Ollila, and M. Muma, *Robust Statistics for Signal Processing*. Cambridge University Press, 2018.

A. Alvera-Azcárate, D. Sirjacobs, A. Barth, and J.-M. Beckers, “Outlier detection in satellite data using spatial coherence,” *Remote Sensing of Environment*, vol. 119, pp. 84–91, 2012.

D. C. Montgomery, *Introduction to Statistical Quality Control*, 6th ed. John Wiley & Sons, Inc., 2009.

P. Whittle, “On stationary processes in the plane,” *Biometrika*, vol. 41, no. 3/4, pp. 434–449, 1954.

M. S. Bartlett, “Physical nearest-neighbour models and non-linear time-series,” *Journal of Applied Probability*, vol. 8, no. 2, pp. 222–232, 1971.

H. G. Malamiri, I. Rousta, H. Olafsson, H. Zare, and H. Zhang, “Gap-filling of MODIS time series land surface temperature (LST) products using singular spectrum analysis (SSA),” *Atmosphere*, vol. 9, no. 9, p. 334, 2018.

V. Dumoulin and F. Visin, “A guide to convolution arithmetic for deep learning,” *arXiv*, no. arXiv:1603.07285, 2016.

References VI

- R Core Team, *R: A Language and Environment for Statistical Computing*, R Foundation for Statistical Computing, Vienna, Austria, 2018. [Online]. Available: https://www.R-project.org/
- R. J. Hyndman, *forecast: Forecasting functions for time series and linear models*, R package version 8.0 ed., 2017. [Online]. Available: http://github.com/robjhyndman/forecast
- R. S. Lunetta, J. F. Knight, J. Ediriwickrema, J. G. Lyon, and L. D. Worthy, “Land-cover change detection using multi-temporal MODIS NDVI data,” *Remote Sensing of Environment*, vol. 105, no. 2, pp. 142–154, 2006.
- K. Prabhakara, W. D. Hively, and G. W. McCarty, “Evaluating the relationship between biomass, percent groundcover and remote sensing indices across six winter cover crop fields in maryland, united states,” *International Journal of Applied Earth Observation and Geoinformation*, vol. 39, pp. 88–102, 2015.
- Q. Yuan, Q. Zhang, J. Li, H. Shen, and L. Zhang, “Hyperspectral image denoising employing a spatial–spectral deep residual convolutional neural network,” *IEEE Transactions on Geoscience and Remote Sensing*, vol. 57, no. 2, pp. 1205–1218, 2019.

Obrigado.

sites.google.com/site/fabiobayer

bayer@ufsm.br